SAND2019-5864C

Effects of Photovoltaic Module Materials and Design on Module Deformation Under Load

James Y. Hartley[1], Ashley Maes[1], Michael Owen-Bellini[2], Thomas Truman[3], Edmund Elce[3], Allan Ward[3], Tariq Khraishi[4], Scott Roberts[1]

[1]Sandia National Laboratories, Albuquerque, NM, USA, 87185; [2]National Renewable Energy Laboratory, Golden, CO, USA, 80401; [3]First Solar Inc., Perrysburg, OH, USA, 43551, [4]University of New Mexico, Albuquerque, NM, USA, 87131

***Abstract* — Finite element models of an aluminum-framed crystalline silicon (c-Si) photovoltaic (PV) module and a glass-glass thin film PV module were constructed and validated against experimental measurements of deflection under uniform pressure loading. Parametric analyses using Latin Hypercube Sampling (LHS) were performed to propagate simulation input uncertainties related to module material properties, dimensions, and manufacturing tolerances into expected uncertainties in simulated deflection predictions. This exercise verifies the applicability and validity of finite element modeling for predicting mechanical behavior of solar modules across architectures and enables computational models to be used with greater confidence in assessment of module mechanical stressors and design for reliability. Sensitivity analyses were also performed on the uncertainty quantification data sets using linear correlation coefficients to elucidate the key parameters influencing module deformation. This information has implications on which materials or parameters may be optimized to best increase module stiffness and reliability, whether the key optimization parameters change with module architecture or loading magnitudes, and whether parameters such as frame design and racking must be replicated in reduced-scale reliability studies to adequately capture full module mechanical behavior.**

***Index Terms* — Finite element modeling, mechanical load, simulation, uncertainty quantification, validation**

I. Introduction

Photovoltaic (PV) modules are routinely subjected to mechanical pressure loading within deployment environments, from exposures to wind and snow. The importance of withstanding these loads is well recognized, with multiple mechanical loading tests built into module qualification standards [1] and cyclic deformation recognized as a driver of component fatigue damage [2]. Despite economic pressure to reduce materials and costs, module deformation under load remains a desirable quantity to minimize.

Computational modeling using the finite element method (FEM) provides a means to analyze mechanical systems without physical hardware, which has significant advantages in parametric optimization and sensitivity analyses of new materials or geometric designs. However, to be utilized with full confidence, models must first be validated against measurable quantities in controlled test cases, to confirm they adequately capture relevant physics prior to being used to explore non-measurable quantities and phenomena. This paper describes the development and validation of finite element models for two PV module design architectures under mechanical pressure loads: an aluminum-framed crystalline silicon (c-Si) module and a glass-glass thin film module. Simulated deformation for each module was compared against experimental measurements, and simulation uncertainties were calculated using Latin Hypercube Sampling (LHS) to propagate material property and module manufacturing uncertainties into predicted deformations. Results were further analyzed to find the input parameters most correlated to module deformation, via linear correlation coefficients.

These results have implications on which module materials or design parameters are impactful candidates for fully characterizing and improving, and which are candidates for cost-cutting. Additionally, many reliability studies are conducted at sub-module scales [3],[4] which necessitates simplification of parameters such as frames and racking with unknown impacts. Developing a full understanding of module behavior enables the representativeness of these sub-module studies to be evaluated and adjusted.

II. Methods

A. Photovoltaic Module Descriptions

The c-Si module in this study had an aluminum framed design with an L-shaped frame cross section and keyed corner fasteners (Fig. 1). The typical laminate structure containing glass, encapsulant, cells, and a backsheet was present, fitted to the frame with an edge tape. Glass thickness was 3.2 mm and planar dimensions were approximately 1.0 m x 1.6 m.

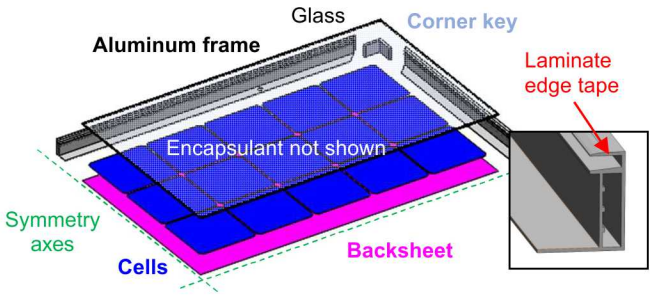

Fig. 1. Quarter-section exploded view of silicon module construction, with inset showing frame cross sectional detail

The glass-glass thin film module had a laminate structure consisting of glass-encapsulant-glass, with an edge seal replacing the perimeter of the encapsulant layer. A semiconducting layer was also present but was of negligible thickness for mechanical analyses. Glass thicknesses were 2.8 mm and 2.2 mm, and approximate planar dimensions were 1.2 m x 2.0 m. The laminate structure was bonded to an under-mount, screwed aluminum frame structure with beads of adhesive.

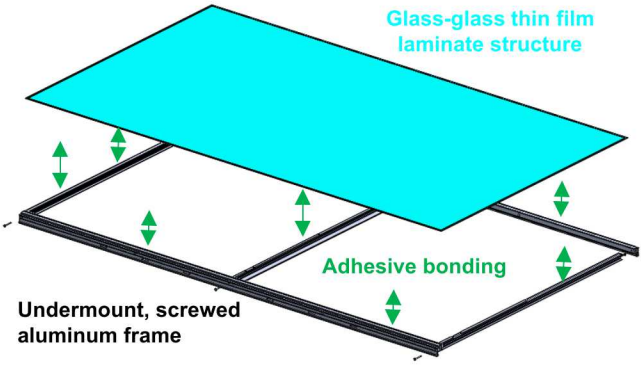

Fig. 2. Glass-glass thin film module construction, showing laminate structure bonded to screwed aluminum frame with adhesive

B. Experimental test cases

Deflection tests were conducted for each module by mounting the module horizontally on a simulated rack structure according to manufacturer specifications and placing weighted bags on the front glass surface to impose a uniform distributed load. Pressures of 1000 Pa and 2400 Pa were applied for the silicon module, with deflections measured along the diagonal relative to a fixed beam. For the glass-glass module, a range of pressures from 1400 to 2800 Pa was imposed, and measurements were taken at key points on the module.

C. Finite Element Models

Finite element models for each module were constructed based on the design definitions, including all the parts shown in Figs. 1 and 2. Small features such as junction boxes, interconnects, and bussing were neglected to save computational cost. Remaining construction details were represented to the best fidelity possible, with frictional surface contact to represent frame interfaces, axial strains applied to model screw tension, and contiguous meshing for adhesive-bonded interfaces. Module mounts were modeled as deformable blocks with an interface area representative of the actual mounting system used. Quarter-symmetry was applicable in both cases.

The applied boundary conditions were uniform pressure loads on the front glass, matching the loads from experimental data. Gravity was included in the same nominal direction as the pressure loads. Figure 3 shows a schematic of applied boundary conditions for a generic module model.

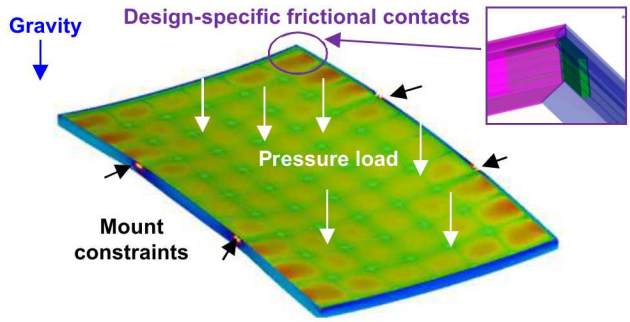

Fig. 3. Schematic of applied model boundary conditions

Room-temperature linear-elastic material behavior was implemented for all module materials (Eqn. 1) with stress σ and strain ε fully described by material elastic modulus E and Poisson's ratio v alone. This was assumed since simulations did not impose temperature variations or incur large strains, and experimental comparison data was collected at temperatures and time scales unlikely for viscous effects to be impactful.

$$\sigma_{ij} = \frac{Ev}{(1+v)(1-2v)}\sigma_{ij}\varepsilon_{kk} + 2\frac{E}{2(1+v)}\varepsilon_{ij} \quad (1)$$

The nominal silicon module consisted of 3,269,894 hexahedral elements, while the nominal glass-glass module consisted of 2,815,988 hexahedral elements, distributed over quarter-symmetric domains. Most parametric geometry changes implemented in this study were captured by adjusting element sizes, and thus total element counts were similar across configurations. Mesh convergence was assessed for nominal module models by halving all element edge lengths (i.e. uniform refinement to 8 times the original element count) and comparing predicted deflections against results from the non-refined mesh, with differences of less than 0.1% in predicted values for the load ranges used.

D. Parametric Materials and Design

To assess influences of module materials and design on deformations under load, LHS was utilized to select sets of input parameter values from plausible ranges. Well-characterized materials with weak temperature dependence such as aluminum assumed uncertainty bounds of ±5% from nominal values, while materials such as polymer adhesives and encapsulants were assigned larger uncertainties to envelope variability in characterization data sets and account for material changes around unrecorded but plausible room temperatures during module loading experiments (e.g. 55-85 °F). Module geometry and construction parameters were varied as well to estimate the effect of assumed process variations and manufacturing tolerances. Parameters and bounds for the glass-glass thin film module and c-Si module are listed in Tables 1 and 2, respectively. Uniform distributions were assumed for all parameters. Details of select geometric parameter implementation for each module model are shown in Figures 4 and 5.

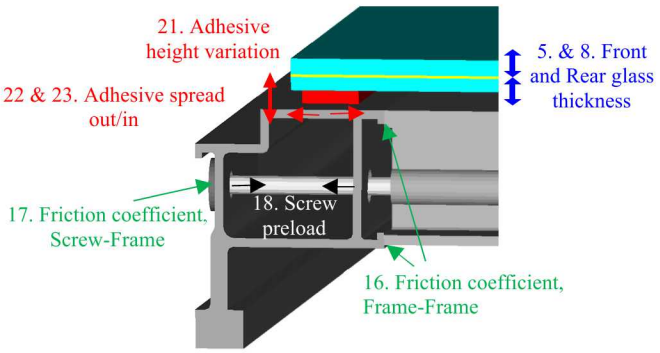

Fig. 4. Implementation of select geometric and boundary condition parameters from Table 1 to glass-glass thin film module model

TABLE 1. UNCERTAIN PARAMETERS AND BOUNDS FOR GLASS-GLASS THIN FILM MODULE MODEL

#	Parameter	Lower Bound	Upper Bound
1	Steel, Elastic Modulus [Pa]	1.8×10^{11}	2.0×10^{11}
2	Steel, Poisson's Ratio	0.276	0.305
3	Front Glass, Elastic Modulus [Pa]	6.2×10^{10}	7.6×10^{10}
4	Front Glass, Poisson's Ratio	0.216	0.264
5	Front Glass Thickness [mm]	2.0	2.4
6	Rear Glass, Elastic Modulus [Pa]	6.2×10^{10}	7.6×10^{10}
7	Rear Glass, Poisson's Ratio	0.216	0.264
8	Rear Glass Thickness [mm]	2.7	2.9
9	Encapsulant, Elastic Modulus [Pa]	1.3×10^{7}	1.9×10^{7}
10	Encapsulant, Poisson's Ratio	0.450	0.499
11	Edge seal, Elastic Modulus [Pa]	2.4×10^{6}	2.8×10^{6}
12	Edge seal, Poisson's Ratio	0.400	0.499
13	Aluminum, Elastic Modulus [Pa]	6.5×10^{11}	7.1×10^{11}
14	Aluminum, Poisson's Ratio	0.314	0.347
15	Frame clamp, Elastic Modulus [Pa]	1.3×10^{8}	2.0×10^{8}
16	Friction coefficient, Frame-Frame	0.2	1.2
17	Friction coefficient, Screw-Frame	0.2	1.2
18	Screw preload artificial strain	-0.001	-0.005
19	Adhesive, Elastic Modulus [Pa]	0.9×10^{6}	2.7×10^{6}
20	Adhesive, Poisson's Ratio	0.400	0.499
21	Adhesive height variation [mm]	-0.5	+1.0
22	Adhesive spread, out, frame 1 [mm]	-2.0	+2.0
23	Adhesive spread, in, frame 1 [mm]	-2.0	+2.0
24	Adhesive spread, out, frame 2 [mm]	-2.0	+2.0
25	Adhesive spread, in, frame 2 [mm]	-2.0	+2.0
26	Adhesive spread, out, frame 3 [mm]	-2.0	+2.0

As shown in Fig. 4, the module laminate is bonded to each frame member via discrete adhesive beads. Each bead was assumed to vary in width along inward (Parameter #23 from Table 1) and outward (#22) spread directions, and similarly on the other frame members (#24-26). Changes to adhesive heights (#21) were made simultaneously on all frame members so the laminate plane would remain parallel to the top of the frame structure. Glass thicknesses (#5 and #8) varied freely without interaction constraints. Frames were secured together via friction at the screw head (#17) and frame-frame interface (#16), with an artificially strained screw (#18) providing a tensile clamping force.

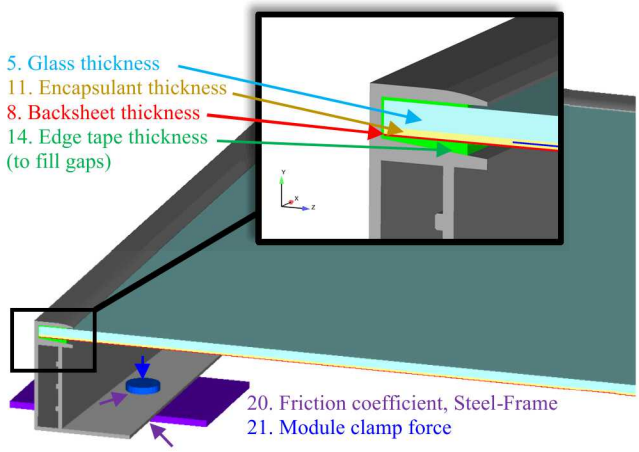

Fig. 5. Implementation of select geometric and boundary condition parameters from Table 2 to c-Si module model

TABLE 2. UNCERTAIN PARAMETERS AND BOUNDS FOR c-Si MODULE MODEL

#	Parameter	Lower Bound	Upper Bound
1	Steel, Elastic Modulus [Pa]	1.8×10^{11}	2.0×10^{11}
2	Steel, Poisson's Ratio	0.276	0.305
3	Glass, Elastic Modulus [Pa]	6.3×10^{10}	7.7×10^{10}
4	Glass, Poisson's Ratio	0.216	0.264
5	Glass Thickness [mm]	3.10	3.30
6	Backsheet, Elastic Modulus [Pa]	1.0×10^{9}	4.0×10^{9}
7	Backsheet, Poisson's Ratio	0.400	0.499
8	Backsheet Thickness [mm]	0.10	0.20
9	Encapsulant, Elastic Modulus [Pa]	1.2×10^{7}	1.8×10^{7}
10	Encapsulant, Poisson's Ratio	0.450	0.499
11	Encapsulant Thickness, total [mm]	0.90	1.00
12	Edge tape, Elastic Modulus [Pa]	1.8×10^{11}	2.0×10^{11}
13	Edge tape, Poisson's Ratio	0.300	0.499
14	Edge tape thickness [mm]*	0.25	0.45
15	Aluminum, Elastic Modulus [Pa]	6.5×10^{11}	7.1×10^{11}
16	Aluminum, Poisson's Ratio	0.314	0.347
17	Silicon, Elastic Modulus [Pa]	1.5×10^{11}	1.9×10^{11}
18	Silicon, Poisson's Ratio	0.252	0.308
19	Friction coefficient, Frame-Frame	0.2	1.2
20	Friction coefficient, Steel-Frame	0.2	1.2
21	Module clamp force [N]	800	1600

** Derived parameter, not independently sampled*

As shown in Fig. 5, the glass (parameter #5 from Table 2), encapsulant (#11), and backsheet (#8) layers could vary in thickness, resulting in a total laminate dimension which was then centered vertically in the frame channel dimension. Silicon cells were also centered within the total encapsulant thickness. The edge tape thickness (#14) was then modified to fill any remaining gap. In this manner, edge tape thickness was not an independently sampled parameter, though sensitivities to its dimension could still be assessed. The module frame was modeled to rest on a steel rail with contact friction (#20), with an additional normal force (#21) imposed by a mounting screw head, which itself was in frictional contact with the frame (#20).

E. Simulations

Parameter selection and propagation into mesh and simulation inputs was conducted using the DAKOTA toolkit at Sandia National Laboratories [5]. Simulations were run in SIERRA/Solid Mechanics. This workflow was scripted for 120 LHS samples for each module, using an incremental approach [5] such that convergence trends could be assessed within subsets of the same hypercube space and additional samples could be added as needed.

III. Results

A. Uncertainty Quantification and Model Validation

To assess model validity against experimental data, mean predicted deflection at select points for each module for the 120 LHS simulations was compared against measured data. Fig. 6 shows results for the c-Si module in terms of deflection across the diagonal when loaded to 1.0 and 2.4kPa. Simulation uncertainty bounds were represented by responses two standard deviations (±2σ) away from the mean, while experimental uncertainty was represented uniformly for each dataset as the largest observed asymmetry between expected symmetric module locations. This was an attempt to represent module-to-module variability based on observed variability in a single module, in the absence of multiple module samples or measurements for deriving a statistically informed uncertainty.

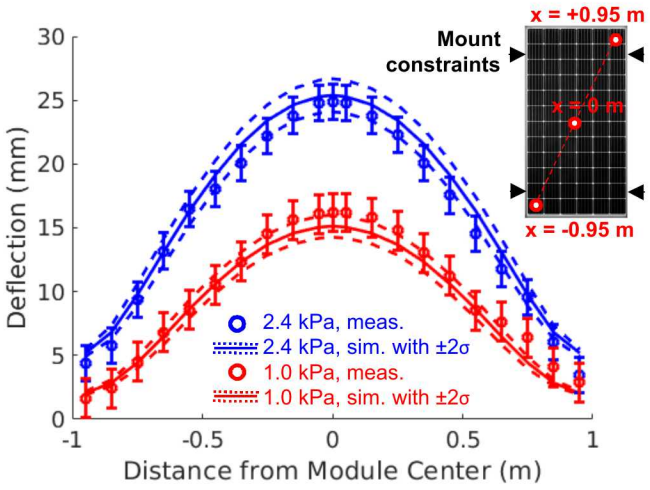

Fig. 6. Measured vs. mean and ±2σ simulated deflection across c-Si module diagonal at 1.0 and 2.4 kPa pressure loads

As shown in Fig. 6, good agreement with experimental measurements was attained for both simulated load cases, with uncertain simulated responses enveloping measurement points. The module showed the largest deflection at the center, decreasing along the diagonal at locations approaching the mounting constraint points. It should be noted that measurement data near the module corners (x = ±0.85-0.95) showed an offset up to approximately 5 mm, despite being near fixed mounting points where no deflection was expected. Since this offset also increased with load magnitude, it was attributed to unexpected deflections in the racking structure. This was propagated to simulation results as a linearly increasing offset to facilitate direct comparisons in predicted module shape.

Simulated deflection from the glass-glass module model were compared against measured deflection at key locations as a function of applied load between approximately 1.4 kPa and 2.8 kPa (Fig. 7). Simulated results are also shown through 0 kPa loading in increments of approximately 0.25 kPa. Like the c-Si module, experimental uncertainty was represented as the largest observed module asymmetry at each load, applied uniformly to all measurement locations for that load. Simulation uncertainty utilized the 120 LHS simulations to derive a standard deviation, with overall simulation uncertainty represented as two standard deviations above and below the mean (±2σ).

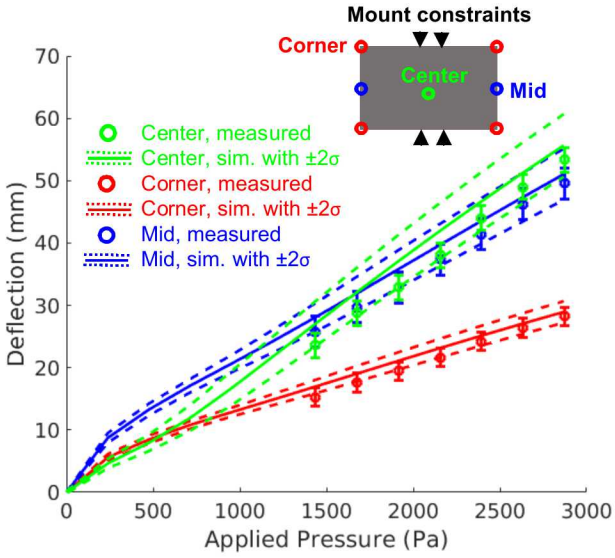

Fig. 7. Measured vs. mean and ±2σ simulated deflections at key points on glass-glass module for pressure loads between 1.4 and 2.8 kPa.

As shown in Fig. 7, satisfactory model agreement was achieved all locations, with average simulation results overestimating deflection but with uncertainties overlapping experimental measurements. The largest deflection was observed at the center and mid edge locations. Inflections in deflection vs. pressure trends can be seen at all locations below approximately 750 Pa simulated load. This is potentially due to frame members shifting upon initial loading, allowing for large apparent displacements at measurement points, before settling into a stable contacted configuration producing the linear load vs. deflection response beyond 750 Pa.

B. Parameter Sensitivity Analysis

Latin hypercube sample data was analyzed for correlations between input parameters and deflection results by computing Pearson's linear correlation coefficient [6] between each input value and predicted deflection magnitude. To demonstrate this

methodology and visualize representative correlation strengths, a plot of sampled input parameters against predicted deflection is shown in Figure 8 for the highest correlated parameter for the c-Si module. Table 3 shows the top five parameters correlated to c-Si module deflection at the center location, under 1.0 kPa and 2.4 kPa applied pressure loads.

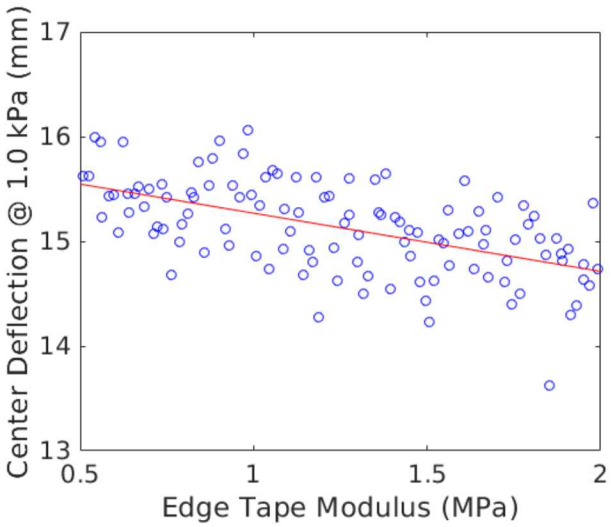

Fig. 8. Sampled values of edge tape elastic modulus vs. predicted deflection at c-Si module center, 1.0 kPa. Trendline included for visualization.

TABLE 3. TOP CORRELATIONS TO c-Si MODULE CENTER DEFLECTION, 1.0 AND 2.4 kPa PRESSURE LOADS

1.0 kPa Pressure Load		2.4 kPa Pressure Load	
Parameter	|R|	Parameter name	|R|
Edge tape modulus	0.630	Glass modulus	0.561
Glass modulus	0.532	Edge tape modulus	0.553
Edge tape Poisson's	0.336	Edge tape Poisson's	0.361
Glass thickness	0.286	Glass thickness	0.321
Encap. thickness	0.132	Encap. thickness	0.111

The top five correlated parameters were consistent between load magnitudes, although a change between edge tape modulus and glass modulus as the top parameter was observed when transitioning between 1.0 and 2.4 kPa loads. This indicates that edge tape modulus is the key parameter allowing deflection upon initial loading, but higher loads eventually overwhelm the material strength such that deflection is then controlled by the higher modulus glass. Both glass modulus and thickness were among top correlated parameters, as expected for a structural module component. Encapsulant thickness also appeared despite being a low modulus material, potentially by contributing to the overall second moment of area of the laminate section rather than by adding substantive material stiffness. However, as the 5th ranked parameter, overall correlation strength was diminishingly low at 0.111 for the 2.4 kPa load case and 0.132 for the 1.0 kPa load case.

For the glass-glass thin film module, correlations to deflection at the module center location were computed at 1.0 kPa and 2.4 kPa loads, with the strongest overall correlation plotted in Figure 9 and the top five parameters for each load shown in Table 4.

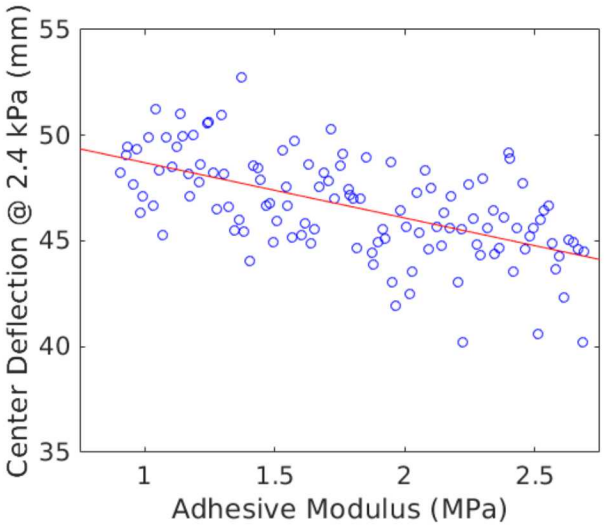

Fig. 9. Sampled values of adhesive elastic modulus vs. predicted deflection at glass-glass module center, 2.4 kPa. Trendline included for visualization.

TABLE 4. TOP CORRELATIONS TO GLASS-GLASS MODULE CENTER DEFLECTION, 1.0 AND 2.4 kPa PRESSURE LOADS

1.0 kPa Pressure Load		2.4 kPa Pressure Load	
Parameter	|R|	Parameter name	|R|
Adhesive modulus	0.557	Adhesive modulus	0.582
Front glass thickness	0.373	Front glass thickness	0.476
Adhesive height	0.363	Adhesive height	0.291
Adhes. spread, frame 3	0.338	Adhes. spread, frame 3	0.280
Aluminum modulus	0.215	Back glass modulus	0.238

Top correlated parameters were consistent between load magnitudes except for the fifth most-correlated parameter, which was back glass modulus at a 2.4 kPa load but changed to aluminum modulus for a 1.0 kPa load. This suggests that laminate construction becomes increasingly influential at large loads, though the small differences and weak overall correlation strengths should be considered in context for this and other conclusions around parameter rankings. However, the presence of three adhesive parameters in the top five most-correlated parameters do suggest that the module response is significantly influenced by both the material itself (adhesive modulus) as well as its application parameters (height and spread variation). Glass properties also appeared as top parameters, as expected for a structural module component.

IV. Conclusions

In this study, full module finite element models for deformation under mechanical pressure loads were validated against experimental test data, including the modeled effects of uncertainties in material and module design parameters. Satisfactory agreement between measured and simulated deformation was observed for a framed c-Si module design as well as a glass-glass thin film module, at multiple comparison locations and load magnitudes between 1 kPa and 2.4 kPa. This exercise provides evidence confirming the applicability of module scale finite element models, allowing such models to be used with greater confidence for design trade studies, environmental scenario analyses, internal stress state analyses, and development of reduced-scale boundary conditions. Additionally, uncertainty quantification and sensitivity studies were conducted using a LHS approach, to inform bounds on simulation prediction uncertainties and on key parameters influential to module deformation.

For both module designs, parameters related to polymeric materials such as adhesives and edge tapes were found to be as correlated to deflection as higher modulus materials more generally associated with module structures, such as glass and aluminum. This suggests that substantive improvements to module stiffness could be attained by optimizing the choice and application of polymer materials, and that fully characterizing the mechanical response of these materials is important to capturing overall module response. Interestingly, module assembly parameters such as friction coefficients and preloads did not appear to be highly influential to predicted module deflection magnitudes, despite being crucial for obtaining modeled to experimental shape agreement. The small angular displacements in frame joints permitted by these interactions appear to be the key phenomena allowing for experimental agreement, with the effect of interaction strength not noticeable once applied pressure reaches 1 kPa.

Finally, it should be noted that the correlations and sensitivities shown herein represent only an abbreviated interpretation of the LHS simulation datasets. Directions for future study could include extending sensitivity analyses to stress quantities, non-linear parameter effects, combined parameter effects, and as functions of load magnitudes and configurations.

Acknowledgements

Sandia National Laboratories is a multi-mission laboratory managed and operated by National Technology and Engineering Solutions of Sandia, LLC., a wholly owned subsidiary of Honeywell International, Inc., for the U.S. Department of Energy's National Nuclear Security Administration under contract DE-NA0003525.

References

[1] R. Arndt and R. Puto. "Basic Understanding of IEC Standard Testing For Photovoltaic Panels". *TÜV SÜD Product Service.* Peabody, Massachusetts. 2010.

[2] N. Bosco *et al*., "Evaluation of Dynamic Mechanical Loading as an accelerated test method for ribbon fatigue," *2013 IEEE 39th Photovoltaic Specialists Conference (PVSC)*, Tampa, FL, 2013, pp. 3173-3178.

[3] M. Owen-Bellini, P. Hacke, S. Spataru, D. C. Miller, and M. D. Kempe, "Combined-Accelerated Stress Testing for Advanced Reliability Assessment of Photovoltaic Modules," *35th European PV Solar Energy Conference and Exhibition,* 2018.

[4] J. Y. Hartley and S. A. Roberts. "Effects of Solar Cell Materials and Geometries on Thermally Induced Interfacial Stresses". *2018 IEEE 45th Photovoltaic Specialists Conference (PVSC),* Waikoloa, HI, 2018, pp. 3179-3184.

[5] B. Adams, M. Ebeida, M. Eldred, et. al. "Dakota, A Multilevel Parallel Object-Oriented Framework for Design Optimization, Parameter Estimation, Uncertainty Quantification, and Sensitivity Analysis: Version 6.8 Theory Manual". *Sandia National Laboratories Report*. SAND2014-4253. Updated May 2018.

[6] A. Haytner. *"Probability and Statistics for Engineers"*. Belmont, CA: Thomson Higher Education. 2007, p. 585.